# Modulation of outer bank erosion by slump blocks: disentangling the protective and destructive role of failed material on the three-dimensional flow structures.

**Authors:**

Christopher Hackney, Geography and Environment, University of Southampton, SO17 1BJ, UK.

Jim Best, Departments of Geology, Geography and GIS, Mechanical Science and Engineering and Ven Te Chow Hydrosystems Laboratory, University of Illinois at Urbana Champaign, Champaign, IL 61820, USA.

Julian Leyland and Stephen E. Darby, Geography and Environment, University of Southampton, SO17 1BJ, UK.

Daniel Parsons, Geography, Earth and Environmental Sciences, University of Hull, HU6 7RX, UK.

Rolf Aalto and Andrew Nicholas, University of Exeter, Geography, Exeter, EX4 4RJ, UK.

Corresponding Author: Christopher Hackney, Geography and Environment, University of Southampton, SO17 1BJ, UK (C.R.Hackney@soton.ac.uk)

**Key Points:**

- Submerged blocks of eroded bank material directly affect the 3-D near-bank flow field
- Submerged slump blocks may deflect flow onto the bank
- A new conceptual model of bank erosion accounts for the influence of submerged slump blocks

**Abstract:**

The 3-dimensional flow field near the banks of alluvial channels is the primary factor controlling rates of bank erosion. Although submerged slump blocks and associated large-scale bank roughness elements have both previously been proposed to divert flow away from the bank, direct observations of the interaction between eroded bank material and the 3-D flow field are lacking. Here we use observations from multibeam echo sounding, terrestrial laser scanning and acoustic Doppler current profiling to quantify, for the first time, the influence of submerged slump blocks on the near-bank flow field. In contrast to previous research emphasising their influence on flow diversion away from the bank, we show that slump blocks may also deflect flow onto the bank, thereby increasing local shear stresses and rates of erosion. We use our measurements to propose a conceptual model for how submerged slump blocks interact with the flow field to modulate bank erosion.

**Index Terms and Keywords:**

1815 EROSION

1825 GEOMORPHOLOGY: FLUVIAL

1856 RIVER CHANNELS

Bank Erosion, Near-bank Flow Field, Bank Roughness, Slump Blocks.

## 1. Introduction

The erosion and deposition of sediment by fluvial bank erosion plays a pivotal role in maintaining the ecological and geomorphological diversity of fluvial channels [*Florsheim et al.*, 2008; *Camporeale et al.*, 2013]. Previous research has shown how the rate at which sediment is exhumed from floodplains by the processes of bank failure, sediment entrainment and transportation, has far reaching implications for geomorphology, ecology, infrastructure management, as well as nutrient and contaminant tracking [e.g. *Marron*, 1992; *Reneau et al.*, 2004; *O'Neal and Pizzuto*, 2011; *Zinger et al.*, 2011]. The intricate relationship between the erosive forces of hydraulic bank erosion (i.e. fluid shear stress) and the 'resistive' forces, as controlled by the lithology and morphology of the bank, make a full appreciation of the flow-form interactions at the river bank a prerequisite to understanding, and predicting, rates of bank erosion.

Past work has highlighted the role of submerged blocks of eroded bank material (henceforth 'slump blocks') in modifying the near-bank flow structure, by providing protective material to the base of the bank [*Thorne,* 1982; *Wood et al., 2001*; Parker et al., *2011*] as well as increasing bank roughness, thereby diverting high velocity flows away from the bank [*Motta et al.*, 2014]. Bank roughness is further enhanced by the bankline topography, which becomes embayed as bank failures occur [*Kean and Smith*, 2006a, 2006b]. In studies of bank erosion within actively migrating meandering channels, recent research has proposed that cohesive slump blocks may serve to armour the underlying non-cohesive bed and thus reduce bank erosion [*Dulal et al.*, 2010; *Parker et al.*, 2011; *Asahi et al.*, 2013; *Eke et al.*, 2014]. *Parker et al.* [2011] argue that subsequent breakdown of the slump blocks may diminish protection of the river bank and lead to renewed bank failure and slumping. *Motta et al.* [2014] also find that slump blocks may protect the bank from erosion, with slump block size, bank height and slope, river bed topography and the presence/type of vegetation potentially controlling their influence on the near-bank processes. However, as detailed observations of the 3-D flow field around, and through, these roughness elements are currently lacking, these models remain largely untested.

Although past studies have investigated the effect of bank roughness on near-bank flows, these have either been of insufficient spatial resolution to resolve fully the three-dimensional flow near the bank [*Jin et al.*, 1990; *Thorne and Furbish*, 1995], or they have documented

flow associated with large-scale roughness elements in physical experiments [*Mizumura and Yamasaka*, 2002; *McCoy et al.*, 2007, 2008; *Yossef and de Vriend*, 2011] and numerical models [*Mcbride et al.*, 2007; *Blanckaert et al.*, 2010, 2012, 2013; *Abad et al.*, 2013], or studied the effects of artificial bend-way weirs, wing-dykes and groynes [*Abad et al., 2008*; *Jamieson et al.*, 2011]. The current absence of detailed 3-D measurements documenting the effects of bank roughness on near-bank flow in natural channels is partly due to the complexity and spatial scale of the processes involved, and remains a significant research gap [*Motta et al.,* 2014]. Resolving the 3-D flow field and obtaining high-resolution topographic data at the scale of the roughness elements in the near-bank region has long been a challenge. However, recent advances in acoustic Doppler profiling [*Kostaschuk et al.*, 2005; *Szupiany et al.*, 2007, 2009; *Vermeulen et al.*, 2014], and high-resolution topographic data collection [*Parsons et al.,* 2005; *Aalho et al.*, 2009; *Nittrouer et al.,* 2011; *Lotsari et al.*, 2014; *Kasvi et al.*, 2015; *Leyland et al.*, 2015] now enable the instantaneous flow and morphology of the near-bank region to be fully quantified, allowing for the novel investigation of these complex process-form interactions.

Herein, we report on unique data from the Mekong River, Cambodia, obtained using a suite of high-resolution topographic (terrestrial laser scanner and multibeam echo sounder) and flow (acoustic Doppler current profiler) instrumentation, that quantify the topography and 3-D flow structure within embayments situated on the outer bank of a large meander bend. Our data reveal, for the first time, the complex flow-form interactions that occur around these large-scale roughness elements and highlight how slump blocks may initially enhance bank erosion, through their steering of the 3-D flow field, before the role of larger bank embayments and large-scale outer bank flow separation act to reduce erosion rates. We use our observations to propose a new conceptual model for the role of bank roughness in controlling the evolution of bankline topography and hence modulating rates of bank erosion.

## 2. Study Site

We present observations from the outer bank of a meander bend (radius of curvature ~ 3,500 m) on the Mekong River, Cambodia (Figure 1). The Mekong River ranks 12$^{th}$, globally, in terms of its length (4900 km) and tenth in terms of its mean annual runoff [475 km$^3$; *Mekong River Commission*, 2005]. This runoff drives a mean annual sediment load of *c.* $1.6\times10^8$ t [*Milliman and Meade*, 1983] The study site is located in a reach that migrates freely across

largely Quaternary alluvium [*Gupta and Liew*, 2007; *Kummu et al.*, 2008; *Carling*, 2009]. The banks at the study site are between 15 – 20 m in height, locally reaching up to 30 m, are formed of homogenous, erodible, unconsolidated, silty, alluvium ($D_{50}$ = 6.2 μm), with the critical shear stress of the bank material being 0.6 N $m^{-2}$ ($\sigma$ = 0.3 N $m^{-2}$, see Supplementary Information for more details of how this estimate was obtained).

## 3. Methods

Measurements of the bank and near-bank topography, for both the submerged and emergent portions of the banks, were made simultaneously from a vessel using a Reson SeaBat 7125SV Multibeam Echo Sounder (MBES) and a Leica P20 Terrestrial Laser Scanner (TLS). Briefly, both instruments were located together spatially and temporally using a Leica 1230 differential Global Positioning System (dGPS) in Real Time Kinematic (RTK) mode, which produced an accuracy in relative position (dGPS base station to vessel antenna) of ±0.02 m in the horizontal and vertical positions. The dGPS was coupled to an Applanix POS-MV WaveMaster Inertial Motion Unit (IMU) that also provided full, real-time, 3-D motion and heading data correction for both MBES and TLS, along with the synchronisation of all survey data streams using the dGPS time stamp and a pulse per second (PPS) signal. The survey data were synchronised and collected using QPS Quality Integrated Navigation System (QINSy) software. Post-survey calibration and correction for angular offsets and the application of sound velocity corrections were applied to the MBES data within CARIS-HIPS software.

Simultaneous with the topographic survey, detailed 3-D flow fields of the near-bank flow structure were measured using an RDI Teledyne 600 kHz acoustic Doppler current profiler (aDcp) deployed from a second vessel. Flow measurements were conducted along a series of short (200 m; ~0.2 of a channel width) transects set perpendicular to the average bank curvature (Figure 1C, and see supporting information, Figure S4, for more details). All flow surveys were conducted when the discharge was 23,000 $m^{-3}$ $s^{-1}$ (Figure 1A). The aDcp was coupled to the same RTK dGPS used in the topographic surveys to provide both position and velocity corrections of the survey vessel. Four passes were recorded along each transect to allow the time-averaged flow structure to be assessed [*Szupiany et al.,* 2007], with individual passes giving an indication of the shorter-term, 'instantaneous', flow structure. The aDcp data were processed in the Velocity Mapping Toolbox [VMT; *Parsons et al.*, 2013]. The resultant mean transects were then rotated using the method of *Rozovskii* [1957] that has been shown

167 to capture well details of the primary and secondary flow fields in a range of complex
168 channel planforms [*Rhoads and Kenworthy*, 1995; *Lane et al.*, 2000; *Szupiany et al.*, 2009].
169
170 **4. Observations**

171 Our MBES and TLS surveys reveal that a series of distinct embayments and slump blocks
172 dominate the subaqueous near-bank topography (Figures 1C, D and E). These features can be
173 up to 200 m in downstream length and 70 m in across-stream width (Figure 1C). Slump block
174 size ranges from 20 × 15 × 10 m (across-stream × downstream × height dimensions) down to
175 blocks that are only decimeters in size, creating a complex assemblage of roughness elements
176 both near to the bank and extending out to *c.* 50 meters from the bankface. It is noticeable
177 that some slump blocks are relatively smaller than others, and that the failed material is
178 located closer to the bank toe some embayments. This is due to the greater exposure of older
179 failed material to extended periods of geomorphologically effective flow during which the
180 blocks are trimmed and material is removed from the bank toe [*Wood et al.* 2001].
181
182 Observations of the 3-D flow field from within an embayment (159 m in downstream length
183 and 28 m in across-stream width) with a large slump block (Embayment 1, slump block
184 circled in Figure 1D) highlight the dominance of both recirculating, separated, flow
185 downstream of the upstream point of the embayment (Figure 2A) and upwelling, bank-
186 directed, flow around the large slump block itself (Figure 2C). It is noted (Figure 2 B and C)
187 that the slump block is located at the outer edge of the recirculation zone that has formed in
188 the embayment. Time-averaged aDcp data reveal that recirculating flow (of *c.* -0.4 m $s^{-1}$) is
189 created within the embayment. Flow at the surface recirculates within the embayment and
190 reattaches to the bank near the downstream limit of the embayment. In addition, flow is
191 steered towards the bank by the large slump block that generates an upwelling in its
192 downstream leeside (Figure 2B and C). Time-averaged smoothed aDcp data highlights
193 upwelling (0.25 m $s^{-1}$) over the slump block (Figure 2C), although instantaneous upwelling,
194 captured in an individual aDcp cross-section, may reach up to 0.4 m $s^{-1}$ (see supporting
195 information, Figure S5). Flow is seen to be diverted strongly towards the bank in the lee of
196 the slump block, with bank-ward flow velocities of 0.3 m $s^{-1}$ (Figure 2B). At this embayment,
197 flow is thus beginning to form a near-bank dead zone where flow velocities are lower (-0.4 m
198 $s^{-1}$ near the bank compared to 2 m $s^{-1}$ at a distance of ~200 m away from the bank) and thus
199 may serve to reduce the rates of bank erosion. However, at the downstream termination of

this flow separation zone, both flow reattachment and flow steering by the slump block bring high velocity fluid inwards toward the bank, generating upwelling and yielding higher boundary shear stresses in the lee-side of the slump block (Figure 3A). The combined effects of flow reattachment from large-scale recirculation in the evolving embayment and topographic steering of flow around the slump block therefore focus the location of erosion at the downstream limit of the embayment, suggesting that the embayment will continue to enlarge and migrate in the downstream direction.

Conversely, observations of the 3-D flow field from within an embayment (114 m in downstream length and 24 m in across-stream width) without failed material at the bank toe (Embayment 2; Figure 1E) reveal that the flow is dominated solely by recirculating flow. The zone of recirculating flow encompasses the entire length and width of the embayment (Figure 2D) and, although the upstream flow in this recirculation zone is similar in magnitude to that observed in Embayment 1, instantaneous maximum recirculating flow velocities were recorded of -0.8 m $s^{-1}$ compared to -0.4 m $s^{-1}$, thus providing an extensive area of low velocities that may serve to decrease boundary shear stresses (Figure 3B). The reattachment point is located at the downstream limit of the embayment, and here higher boundary shear stresses are present as flow impinges against the bank (Figure 3B). It is noted that this embayment is located downstream of a series of embayments (Figure 1C), and there may thus be some flow inheritance and influence on the primary and secondary flow. The lack of failed material in the subaqueous topography results in lower magnitude (relative to Embayment 1) vertical velocities (Figure 2F), both in the time-averaged (0.1 m $s^{-1}$ compared to 0.25 m $s^{-1}$) and instantaneous (0.2 m $s^{-1}$ compared to 0.4 m $s^{-1}$) aDcp cross-sections (see supporting information, Figure S6). The reduced magnitude and extent of this near-bank upwelling reduces boundary shear stresses when compared to those experienced in the presence of a slump block (Figure 3).

## 5. Discussion

The application of high-resolution 3-D flow and topographic survey techniques to bank embayments at different stages of their evolution has revealed the influence that slump blocks may have upon the instantaneous near-bank flow field. Our observations reveal that, at certain phases during the lifetime of slump blocks, the near-bank flow field may be deflected up and over the block and towards the bank, thereby promoting erosion. In a similar way,

observations have shown that flow may be deflected up and over bendway weirs and groynes at certain flow stages [*Abad et al.* 2008; *McCoy et al.*, 2008; *Bhuiyan et al.*, 2010; *Jamieson et al.*, 2011; *Yossef and de Vriend*, 2011]. *Abad et al.* [2008] found that flow over submerged bendway weirs at bankfull and half bankfull stage steered flow over these structures, accelerating flow around them and leading to higher shear velocities due to flow acceleration over, and fluid shear from, the tips of the weirs (by way of comparison, our study was conducted at half the bankfull discharge). *Abad et al.* [2008] also found that although such weirs could help reduce bank erosion by reducing basal scour, flow around the weirs at higher flow stages could promote bank retreat due to increased shear stresses on the bank produced by the weir flow field. These results find similarities in the slump block flow fields revealed herein.

Previous treatments of slump blocks in models of outer bank erosion and channel migration have been grounded in a 1-D/2-D representation of the role that roughness plays in diverting the high velocity core away from the bank through the influence of form drag [*Kean and Smith*, 2006a, 2006b], as well as the protective role of failed material at the bank toe [*Parker et al.* 2011; *Motta et al,* 2014]. These approaches have led to a treatment of the armouring afforded by failed material within models of meandering river migration, such that as the block disintegrates, the level of protection provided to the bank toe decreases linearly [e.g. *Parker et al.* 2011]. Indeed, *Eke et al.* [2014] highlight that an explicit treatment of the role that slump blocks play in influencing bank shear stresses is missing from the current model of *Parker et al.* [2011]. The data presented herein demonstrates that such a relationship may be more complex than current representations of this phenomenon suggest, in that at different periods of slump block evolution, near-bank shear stresses may be increased, as well as decreased, as a direct result of blocks of failed material. Although in some configurations early in their life-cycle, slump blocks may deflect high-velocity cores away from the bank, thus reducing bank shear stresses [*Kean and Smith*, 2006a, 2006b; *Parker et al.*, 2011], our results show that once the block has been trimmed sufficiently, slump blocks may steer flow up, over, and around their topography and onto the adjacent bank. This flow deflection increases boundary shear stresses, focusing erosion onto the downstream end of the block and near the end of the bank embayment. We note this mechanism may also occur where slump blocks exist in the absence of embayments and that additional further studies are required at a range of spatial scales to ascertain whether this behaviour is scale-dependent. Such effects also find parallels in the recent work of *Abad et al.* [2013] who document the influence of

267 migrating bedforms on bank shear stresses. A fruitful avenue for future studies will be to
268 better quantify the turbulent fluxes and Reyonlds stresses associated with these slump block
269 effects. Nevertheless, such flow-steering due to slump block topography has clear
270 implications for the rate, and location, of erosion as represented in numerical models of bank
271 erosion.
272
273 The present study thus highlights the need to better constrain the role that slump blocks and
274 embayments play in bank erosion, since these roughness elements play a key role in
275 determining the rates and mechanisms of channel migration through their role in driving
276 chute cut-offs [*Markham and Thorne*, 1992; *Constantine et al.*, 2010; *Grenfell et al.*, 2012]
277 and moderating rates of bank erosion [*Kean and Smith*, 2006a, 2006b; *Darby et al.*, 2010;
278 *Leyland et al.*, 2015]. Our results now enable the added complexity of form-flow interactions
279 produced by the presence of slump blocks to be incorporated into these models. To this end,
280 we propose a new conceptual model for the evolution of river bank embayments (Figure 4)
281 that accounts for both the protective role afforded by slump blocks in their early stages, and
282 the enhanced erosion they may induce due to topographic steering at later stages of their
283 evolution.
284
285 During Stage I (Figure 4), a single, or series of, bank failures causes the formation of the
286 initial embayment, and the deposition of failed material at the bank toe. At this stage, the high
287 velocity core is deflected away from the bank toe by the failed material and planform
288 geometry of the embayment, thus affording protection to the bank. In Stage II, hydraulic
289 forces act to erode and trim the slump block. Although form roughness induced by the larger
290 planform of the bank continues to deflect high velocity cores away from the bank,
291 topographic steering of the near-bank flow causes flow to move over, and around, the block,
292 generating bank-directed flow. This flow steering causes higher shear stresses to be exerted
293 on the bank and leads to downstream enlargement of the embayment. Erosion also occurs due
294 to the high shear stresses present in the reattachment region of the flow separation zone
295 formed within the embayment. Stage III sees growth of the embayment, and the continued
296 disintegration of the slump block, with further slumps adding to erosion as in Stage II. The
297 embayment grows in size, increasing form drag, until it generates a sustained large zone of
298 recirculating, separated, flow that is larger than any new slumps that move into this region.
299 Slower flow within the majority of the larger flow separation region produces lower
300 velocities, which lessen bank erosion, with erosion now principally occurring at the

downstream end of the embayment. Finally, Stage IV sees the embayment size stabilise due to large-scale flow separation protecting the bank from significant further erosion. The development of upstream embayments, formed from new slumps, may propagate downstream, and subsume the original embayment, returning the bankline to a pre-embayment planform.

In summary, the role of submerged slump blocks in modulating the near-bank 3-D flow field is far more complex than previously thought. Failed material may act to both protect the bank from erosion as proposed in past work [*Wood et al. 2001; Parker et al.*, 2011; *Motta et al. 2014*], but may also enhance bank erosion by deflecting flow up, and onto, the bank as the geometric properties of the slump block change. It is thus clear that in order to develop better predictive models of bank erosion, all of these effects must be considered, and that future work needs to parameterize the influence of slump block flow-form interactions at different stages of embayment evolution. Although the present results illustrate one case example, our novel data suggest the possible differential influences of slump blocks at various times in their life cycle. Further research is needed to constrain these process dynamics across a range of flow stages that determine the magnitude and distribution of shear stress [*Papanicolaou et al.* 2007; *Guo and Julien*, 2009; *Nikora and Roy,* 2012]. Additionally, more work is needed to quantify the effects of slump block size, orientation, shape and position relative to the bank, and their role in enhancing or reducing bank erosion, in a similar way to past studies of flow around groynes and bendway weirs [*Przedwojski*, 1995; *Abad* et al., 2008].

## 6. Acknowledgements

This research was supported by awards NE/JO21970/1, NE/JO21571/1 and NE/JO21881/1 (to Southampton, Exeter and Hull, respectively) from the UK Natural Environment Research Council (NERC). JB was in receipt of a Diamond Jubilee Fellowship from the University of Southampton and a National Great Rivers Research and Education Center (NGRREC) Faculty Fellowship that facilitated the writing of this paper. All data is available on request from the corresponding author. We thank the Mekong River Commission and Department for Hydrology and Water Resources in Cambodia for logistical support. We thank Mark Dover of the Cartographic Unit, Geography and Environment, University of Southampton for his help in producing Figure 4. The comments of the editor and two reviewers greatly improved the quality of the manuscript.

## 7. References


Aalho, P., A. Hyyppa, H. Kaartinen, J. Hyyppa, and A. Jaakkola (2009), Application of boat-based laser scnning for river survey, *Earth Surf. Process. Landforms*, *34*, 1831 – 1838, doi:10.1002/esp.1879.

Abad, J. D., B.L. Rhoads, I. Güneralp, and M. H. Garcia (2008), Flow strcuture at different stages in a meander-bend with bendway weirs, *Journal of Hydrauic Engineering*, 134, 1052-1063.

Abad, J. D., C. E. Frias, G. C. Buscaglia, and M. H. Garcia (2013), Modulation of the flow structure by progressive bedforms in the Kinoshita meandering channel, *Earth Surf. Process. Landforms*, *38*(13), 1612 - 1622, doi:10.1002/esp.3460.

Asahi, K., Y. Shimizu, J. Nelson, and G. Parker (2013), Numerical simulation of river meandering with self evolving banks, *J. Geophys. Res. - Earth Surf.*, *118*, 22082229, doi:10.1002/jgrf.20150.

Bhuiyan, F., R. D. Hey, and P. R. Wormleaton (2010), Bank-Attached Vanes for Bank Erosion Control and Restoration of River Meanders, *J. Hydraul. Eng.*, *136*(9), 583–596, doi:10.1061/(ASCE)HY.1943-7900.0000217.

Blanckaert, K., A. Duarte, and A. J. Schleiss (2010), Influence of shallowness, bank inclination and bank roughness on the variability of flow patterns and boundary shear stress due to secondary currents in straight open-channels, *Adv. Water Resour.*, *33*(9), 1062–1074, doi:10.1016/j.advwatres.2010.06.012.

Blanckaert, K., A. Duarte, Q. Chen, and A. J. Schleiss (2012), Flow processes near smooth and rough (concave) outer banks in curved open channels, *J. Geophys. Res.*, *117*(F4), F04020, doi:10.1029/2012JF002414.

Blanckaert, K., M. G. Kleinhans, S. J. McLelland, W. S. J. Uijttewaal, B. J. Murphy, A. van de Kruijs, D. R. Parsons, and Q. Chen (2013), Flow separation at the inner (convex) and outer (concave) banks of constant-width and widening open-channel bends, *Earth Surf. Process. Landforms*, *38*(7), 696–716, doi:10.1002/esp.3324.

Camporeale, C., E. Perucca, L. Ridolfi, and A. M. Gurnell (2013), Modeling the interactions between river morphodynamics and riparian vegetation, *Rev. Geophys.*, doi:10.1002/rog.20014.

Carling, P. A. (2009), The geology of the Lower Mekong River, in *The Mekong: Biophysical environment of an international river basin*, pp. 13–28.

Commission, M. R. (2005), *Overview of the Hydrology of the Mekong River Basin*, Vientiane, Laos.

Constantine, J. A., S. R. McLean, and T. Dunne (2010), A mechanism of chute cutoff along large meandering rivers with uniform floodplain topography, *Bull. Geol. Soc. Am.*, *122*(5-6), 855–869, doi:10.1130/B26560.1.

Darby, S. E., H. Q. Trieu, P. A. Carling, J. Sarkkula, J. Koponen, M. Kummu, I. Conlan, and J. Leyland (2010), A physically based model to predict hydraulic erosion of fine-grained riverbanks: The role of form roughness in limiting erosion, *J. Geophys. Res.*, *115*(F4), 1–20, doi:10.1029/2010JF001708.

Dulal, K. P., K. Kobayashi, Y. Shimizu, and G. Parker (2010), Numeircal computation of free meandering channels with the application of slump blocks on the outer bends, *J. Hydro-environment Res.*, *3*(4), 239–246, doi:10.1016/j.jher.2009.10.012.

Eke, E., G. Parker, and Y. Shimizu (2014), Numerical modelling of erosional and depositional bank processes in migrating river bends with self-formed width: Morphodynamics of bar push and bank pull, *J. Geophys. Res. Earth Surf.*, (119), 1455–1483, doi:10.1002/2013JF003020.Received.

Florsheim, J. L., J. F. Mount, and A. Chin (2008), Bank erosion as a desirable attribute of rivers, *Bioscience*, *58*(6), 519 – 529.

Grenfell, M. C., R. Aalto, and A. Nicholas (2012), Chute channel dynamics in large, sand-bed meandering rivers, *Earth Surf. Process. Landforms*, *37*(3), 315–331, doi:10.1002/esp.2257.

Guo, J., and P.Y. Julien (2009) Shear stress in smooth rectangular open-channel flows, *Journal of Hydraulic Engineering*, 131, 1, 30 - 37. doi:10.1061/(ASCE)0733-9429(2005)131:1(30).

Gupta, A., and S. C. Liew (2007), The Mekong from satellite imagery: A quick look at a large river, *Geomorphology*, *85*(3-4), 259–274, doi:10.1016/j.geomorph.2006.03.036.

Jamieson, E. C., C. D. Rennie, R. B. Jacobson, and R. D. Townsend (2011), 3-D flow and scour near a submerged wing dike: ADCP measurements on the Missouri River, *Water Resour. Res.*, *47*(7), 1–20, doi:10.1029/2010WR010043.

Jin, Y. C., P. M. Steffler, and F. E. Hicks (1990), Roughenss effects on flow and shear-stress near outside bank of curved channel, *J. Hydraul. Eng.*, *116*(4), 563 – 577, doi:10.1061/(ASCE)0733-9429(1990).

Kasvi, E., M. Vaaja, H. Kaartinen, A. Kukko, A. Jaakkola, C. Flener, H. Hyyppä, J. Hyyppä, and P. Alho (2015), Sub-bend scale flow–sediment interaction of meander bends — A combined approach of field observations, close-range remote sensing and computational modelling, *Geomorphology*, *238*, 119–134, doi:10.1016/j.geomorph.2015.01.039.

Kean, J. W., and J. D. Smith (2006a), Form drag in rivers due to small-scale natural topographic features: 1. Regular sequences, *J. Geophys. Res.*, *111*(F4), F04009, doi:10.1029/2006JF000467.

Kean, J. W., and J. D. Smith (2006b), Form drag in rivers due to small-scale natural topographic features: 2. Irregular sequences, *J. Geophys. Res.*, *111*(F4), F04010, doi:10.1029/2006JF000490.

Kostaschuk, R., J. Best, P. Villard, J. Peakall, and M. Franklin (2005), Measuring flow velocity and sediment transport with an acoustic Doppler current profiler, *Geomorphology*, *68*(1-2), 25–37, doi:10.1016/j.geomorph.2004.07.012.

Kummu, M., X. X. Lu, A. Rasphone, J. Sarkkula, and J. Koponen (2008), Riverbank changes along the Mekong River: Remote sensing detection in the Vientiane–Nong Khai area, *Quat. Int.*, *186*(1), 100–112, doi:10.1016/j.quaint.2007.10.015.

Lane, S. N., K. F. Bradbrook, K. S. Richards, P. M. Biron, and A. G. Roy (2000), Secondary circulation cells in river channel confluences : measurement artefacts or coherent flow structures ?, *Hydrol. Process.*, *14*, 2047 – 2071.

Leyland, J., S. E. Darby, L. Teruggi, M. Rinaldi, and D. Ostuni (2015), A self-limiting bank erosion mechanism? Inferring temporal variations in bank form and skin drag from high resolution topographic data, *Earth Surf. Process. Landforms*, doi:10.1002/esp.3739.

Lotsari, E., M. Vaaja, C. Flener, H. Kaartinen, A. Kukko, E. Kasvi, H. Hyyppä, J. Hyyppä, and P. Alho (2014), Annual bank and point bar morphodynamics of a meandering river determined by high-accuracy multitemporal laser scanning and flow data, *Water Resour. Res.*, *50*, 5532–5559, doi:10.1002/2013WR014106.Received.

Markham, A. J., and C. R. Thorne (1992), Geomorphology of gravel-bed river bends, in *Dynamics of Gravel-Bed Rivers*, edited by P. Billi, R. D. Hey, C. R. Thorne, and P. Tacconi, pp. 433 – 457, Wiley, Chichester.

Marron, D. C. (1992), Floodplain storage of mine taillings in the Belle Fourche River system: a sediment budget approach., *Earth Surf. Process. Landforms*, *17*, 675 – 685, doi:10.1002/esp.3290170704.

Mcbride, M., W. C. Hession, D. M. Rizzo, and D. M. Thompson (2007), The influence of riparian vegetation on near-bank turbulence : a flume experiment, *Earth Surf. Process. Landforms*, *32*(13), 2019–2037, doi:10.1002/esp.

McCoy, A., G. Constantinescu, and L. Weber (2007), A numerical investigation of coherent structures and mass exchange processes in channel flow with two lateral submerged groynes, *Water Resour. Res.*, *43*(5), 1–26, doi:10.1029/2006WR005267.

McCoy, A., G. Constantinescu, and L. J. Weber (2008), Numerical Investigation of Flow Hydrodynamics in a Channel with a Series of Groynes, *J. Hydraul. Eng.*, *134*(2), 157–172, doi:10.1061/(ASCE)0733-9429(2008)134:2(157).

Milliman, J. D., and R. H. Meade (1983), World-wide delivery of river sediment to the oceans, *J. Geol.*, *91*(1), 1 – 21.

Mizumura, K., and M. Yamasaka (2002), Flow in Open-Channel Embayments, *J. Hydraul. Eng.*, *128*, 1098–1101.

Motta, D., E. J. Langendoen, J. D. Abad, and M. H. García (2014), Modification of meander migration by bank failures, *J. Geophys. Res. Earth Surf.*, *119*(5), 1026–1042, doi:10.1002/2013JF002952.

Nikora, V. and A.G. Roy (2012). Secondary flows in rivers: Theoretical framework, recent advances and current challenges, in *Gravel Bed Rivers: Processes, Tools and Environments 2nd edition*, edited by Church, M., P. Biron and A.G. Roy, pp. 3-23, Wiley and Sons, Hoboken, NJ, USA.

Nittrouer, J. A., D. Mohrig, M.A. Allison and A-P. B. Peyret, (2011), The lowermost Mississippi River: a mixed bedrock-alluvial channel. *Sedimentology*, *58*, 1914–1934. doi: 10.1111/j.1365-3091.2011.01245.x

O'Neal, M. A., and J. E. Pizzuto (2011), The rates and spatial patterns of annual bank erosion revealed through terrestrial laser-scanner surveys of the South River, Virginia., *Earth Surf. Process. Landforms*, *36*(695 - 701), doi:10.1002/esp.2098.

Papanicolaou, A.N., M. Elhakeem and R. Hilldale (2007) Secondary current effects on cohesive river bank erosion, *Water Resources Research,* 43, W12418, doi:10.1029/2006WR005763.

Parker, G., Y. Shimizu, G. V. Wilkerson, E. C. Eke, J. D. Abad, J. W. Lauer, C. Paola, W. E. Dietrich, and V. R. Voller (2011), A new framework for modeling the migration of meandering rivers, *Earth Surf. Process. Landforms*, *36*(1), 70–86, doi:10.1002/esp.2113.

Parsons, D.R., J.L. Best, R.J. Hardy, R. Kostaschuk, S.N. Lane and O. Orfeo, (2005), The morphology and flow fields of three-dimensional dunes, Rio Paraná, Argentina: results from simultaneous multibeam echo sounding and acoustic Doppler current profiling, *J. Geophysical Research, Earth Surface*, 110, F04S03, doi:10.1029/2004JF000231.

Parsons, D. R., P. R. Jackson, J. A. Czuba, F. L. Engel, B. L. Rhoads, K. A. Oberg, J. L. Best, D. S. Mueller, K. K. Johnson, and J. D. Riley (2013), Velocity Mapping Toolbox (VMT): a processing and visualization suite for moving-vessel ADCP measurements, *Earth Surf. Process. Landforms*, *38*(11), 1244 – 1260, doi:10.1002/esp.3367.

Przedwojski, B. (1995), Bed topography and local scour in rivers with banks protected by groynes, *Journal of Hydraulic Research*, 33, 257-273.

Reneau, S. ., P. G. Drakos, D. Katzman, D. V. Malmon, E. V. McDonald, and R. T. Ryti (2004), Geomorphic controls on contaminant distribution along an ephemeral stream, *Earth Surf. Process. Landforms*, *29*, 1209 – 1223, doi:10.1002/esp.1085.

Rhoads, B. L., and S. T. Kenworthy (1995), Flow structure at an asymmetrical stream confluence, *Geomorphology*, *11*(4), 273–293, doi:10.1016/0169-555X(94)00069-4.

Rozovskii, I. L. (1957), Flow of water in bends of open channels, *Akad. Sci. Ukr. SRR*.

Schumm, S. A. (1977), *The Fluvial System*, Wiley, New York.

Szupiany, R. N., M. L. Amsler, J. L. Best, and D. R. Parsons (2007), Comparison of Fixed- and Moving-Vessel Flow Measurements with an aDp in a Large River, *J. Hydrol. Eng.*, *133*, 1299–1309, doi:10.1061/(ASCE)0733-9429(2007)133:12(1299).

Szupiany, R. N., M. L. Amsler, D. R. Parsons, and J. L. Best (2009), Morphology, flow structure, and suspended bed sediment transport at two large braid-bar confluences, *Water Resour. Res.*, *45*(5), n/a–n/a, doi:10.1029/2008WR007428.

Thorne, C.R. (1982), Processes and mechanisms of river bank erosion, in *Gravel-Bed Rivers*, edited by R.D. Hey, J.C. Bathurst, and C.R. Thorne, pp. 227 - 271, Wiley, Chichester, U.K.

Thorne, S. D., and J. D. Furbish (1995), Influences of coarse bank roughness on flow within a sharply curved fiver bend, *Geomorphology*, *12*, 241–257.

Vermeulen, B., M. G. Sassi, and A. J. F. Hoitink (2014), Improved flow velocity estimates from moving-boat ADCP measurements, *Water Resour. Res.*, *50*, 4186–4196, doi:10.1002/2013WR015152.Received.

Wood, A. L., A. Simon, P. W. Downs, and C. R. Thorne (2001), Bank-toe processes in incised channels: The role of apparent cohesion in the entrainment of failed bank materials, *Hydrol. Process.*, *15*(1), 39–61, doi:10.1002/hyp.151.

Yossef, M. F. M., and H. J. de Vriend (2011), Flow details near river groynes: experimental investigation, *J. Hydraul. Eng.*, *137*, 504–516, doi:10.1061/(ASCE)HY.1943-7900.

Zinger, J. A., B. L. Rhoads, and J. L. Best (2011), Extreme sediment pulses generated by bend cut-offs along a large meandering river, *Nat. Geosci.*, *4*, 675–678, doi:10.1038/NGEO1260.

## Figure Captions

**Figure 1: A)** 2014 hydrograph of the Mekong River at Kratie, Cambodia. Surveys were conducted at the time highlighted by the arrow. **B)** Location of the study site on the outer bank of a large meander, located ~150 km downstream of the gauge at Kratie. **C)** The location of flow and topographic datasets used in this study. The yellow lines depict acoustic Doppler current profiler (aDcp) transects, whereas the red line depicts the extent of the

Terrestrial Laser Scanner (TLS) survey undertaken. The shaded box outlines the area covered by the Multibeam Echo Sounding (MBES) survey. The two bank embayments discussed in this paper are highlighted. **D)** Embayment 1 topography, representative of a newly formed embayment. **E)** Embayment 2 topography, which is a more developed (older) embayment. Note the slump block highlighted by the black circle in D), and the lack of failed material along the bank toe in E). Flow is right to left in each of panels D and E.

**Figure 2:** 3D flow structure observed within the bank embayments with slump blocks (Embayment 1: **A-C**) and without slump blocks (Embayment 2: **D-F**). Panels A and C display primary flow velocity (m $s^{-1}$) after rotation following the method of Rozovskii (1957). Streamlines of primary velocity are depicted as white lines in all panels. Panels B and E display cross-stream flow velocity (m $s^{-1}$; where blue is flow into the bank, red is flow away from the bank) as defined by Rozovskii (1957). Panels C and F display vertical flow velocities (m $s^{-1}$) where red is upwelling and blue is downwelling. Note colour scales vary between panels. The black arrows in panels B, C, E and F are cross-stream velocity vectors, scaled by magnitude. The X in panels B and C mark the location of the slump block highlighted in Figure 1 and discussed in the text.

**Figure 3: A)** Boundary shear stress (N $m^{-2}$) derived from the time-averaged aDcp transects within Embayment 1. The grey boxes in Transects 1C and 1D denote the extent of the slump block in the cross-stream dimension (see Figure 1D). The block is located 20 m upstream of Transect 1C and 10 m downstream of Transect 1D. In total, the block is 25 m in downstream length. Note how the location of peak shear stress close to the bank is deflected away from the bank at the entrance to the embayment (transects 1B and 1C), but is located much closer to the bank in transect 1D. A smaller peak in boundary shear stresses occurs in Transect 1F, at the downstream extent of the embayment, due to flow reattachment. **B)** Boundary shear stress (N $m^{-2}$) derived from the time-averaged aDcp transects within Embayment 2 without slump blocks. Note how the distribution of shear stresses close to the bank remains constant in location through the embayment. The peak in boundary shear stresses in Transect 2C, at the downstream extent of the embayment, represents the flow reattachment zone.

**Figure 4:** Conceptual model for the development of a bank embayment, and the role that slump blocks play in diverting flow away from, and on to, the bank at different stages of embayment evolution. The black lines represent streamlines. The dashed lines represent the shear layer.

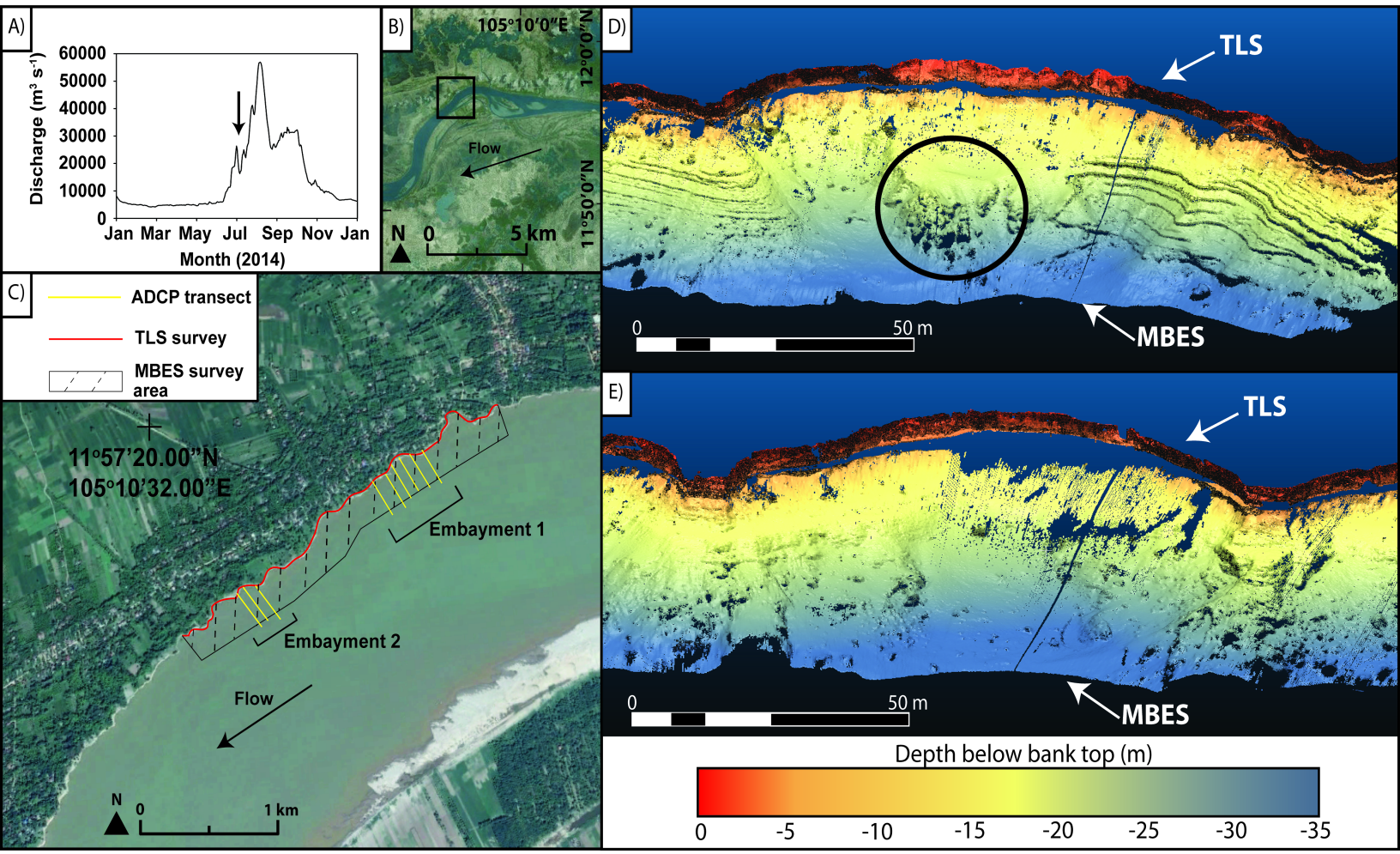
A)
Discharge (m³ s⁻¹)
60000
50000
40000
30000
20000
10000
0
Jan Mar May Jul Sep Nov Jan
Month (2014)
B)
105°10'0"E
12°0'0"N
11°50'0"N
Flow
N
0
5 km
C)
ADCP transect
TLS survey
MBES survey area
11°57'20.00"N
105°10'32.00"E
Embayment 1
Embayment 2
Flow
N
0
1 km
D)
TLS
0
50 m
MBES
E)
TLS
0
50 m
MBES
Depth below bank top (m)
0
-5
-10
-15
-20
-25
-30
-35

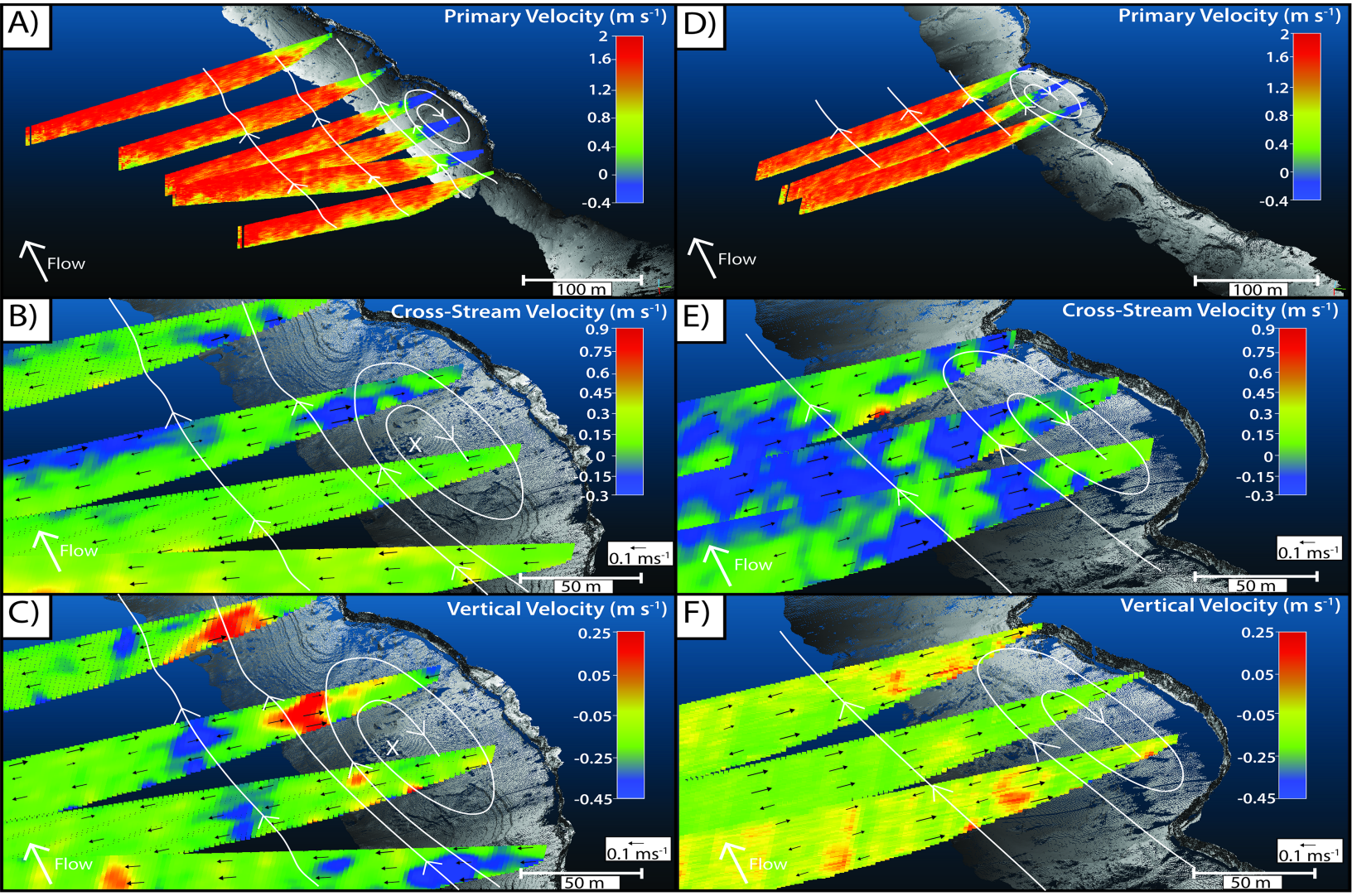
A)
Primary Velocity (m s-1)
2
1.6
1.2
0.8
0.4
0
-0.4
Flow
100 m
D)
Primary Velocity (m s-1)
2
1.6
1.2
0.8
0.4
0
-0.4
Flow
100 m
B)
Cross-Stream Velocity (m s-1)
0.9
0.75
0.6
0.45
0.3
0.15
0
-0.15
-0.3
X
Flow
0.1 ms-1
50 m
E)
Cross-Stream Velocity (m s-1)
0.9
0.75
0.6
0.45
0.3
0.15
0
-0.15
-0.3
Flow
0.1 ms-1
50 m
C)
Vertical Velocity (m s-1)
0.25
0.05
-0.05
-0.25
-0.45
X
Flow
0.1 ms-1
50 m
F)
Vertical Velocity (m s-1)
0.25
0.05
-0.05
-0.25
-0.45
Flow
0.1 ms-1
50 m

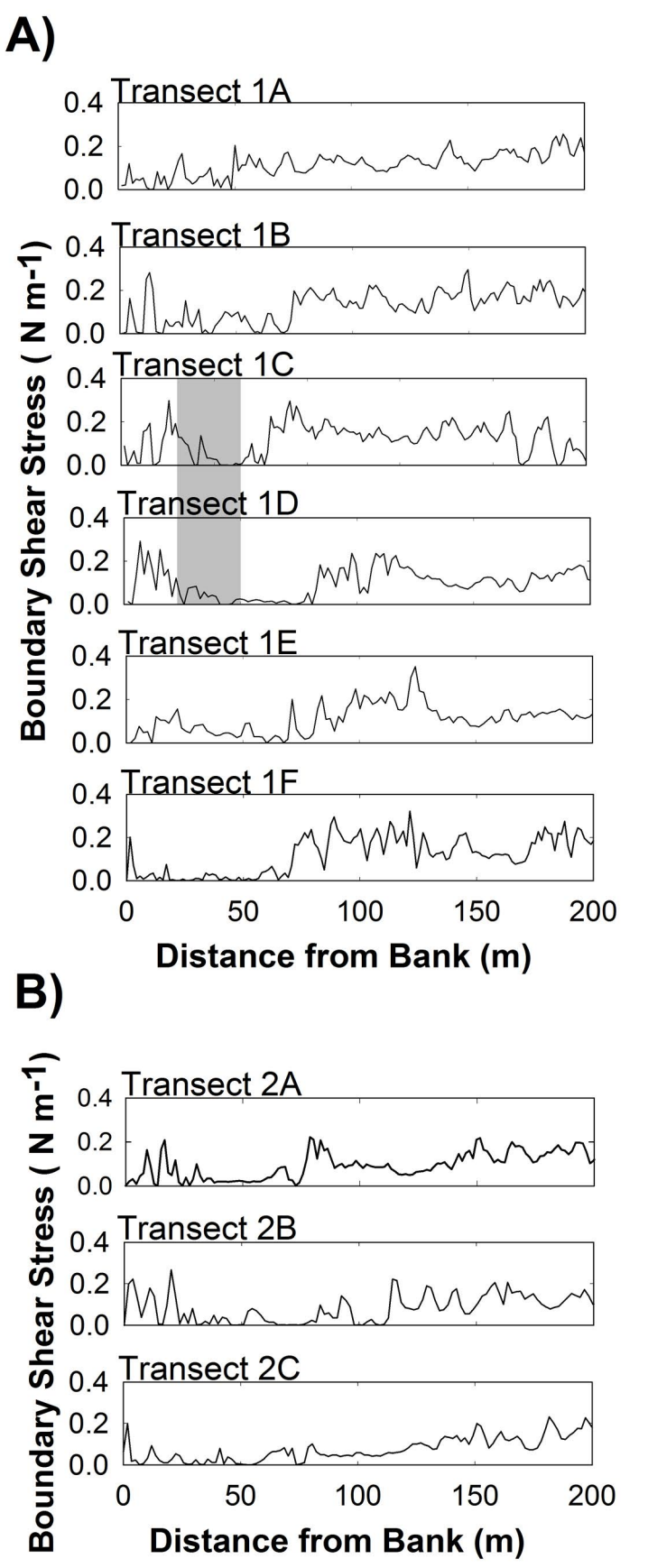
A)
Transect 1A
Transect 1B
Transect 1C
Transect 1D
Transect 1E
Transect 1F
0.4
0.2
0.0
Boundary Shear Stress ( N m-1)
0
50
100
150
200
Distance from Bank (m)
B)
Transect 2A
Transect 2B
Transect 2C
0.4
0.2
0.0
Boundary Shear Stress ( N m-1)
0
50
100
150
200
Distance from Bank (m)

Stage I: Failure and initiation of embayment

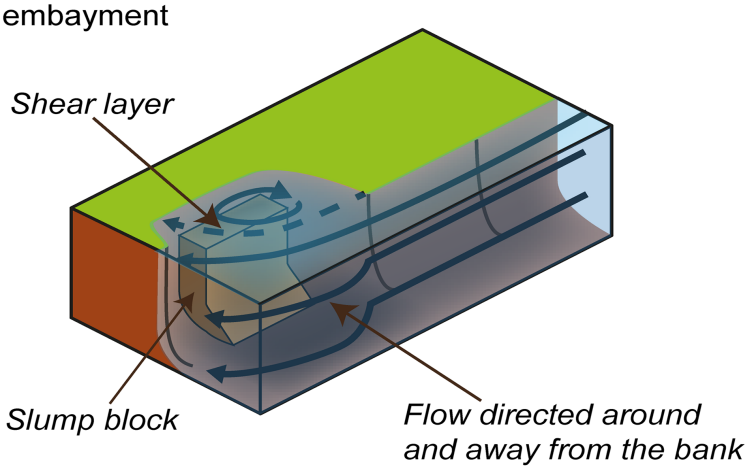


Stage II: Trimming and embayment enlargement

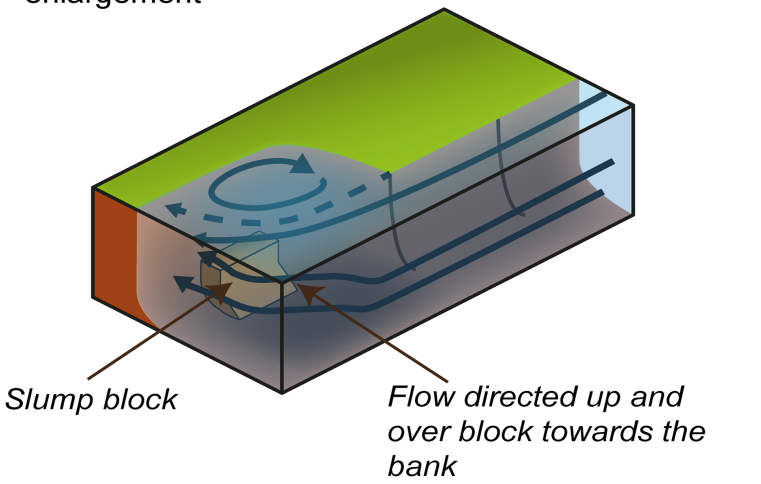


Stage III: Embayment growth and stabilization

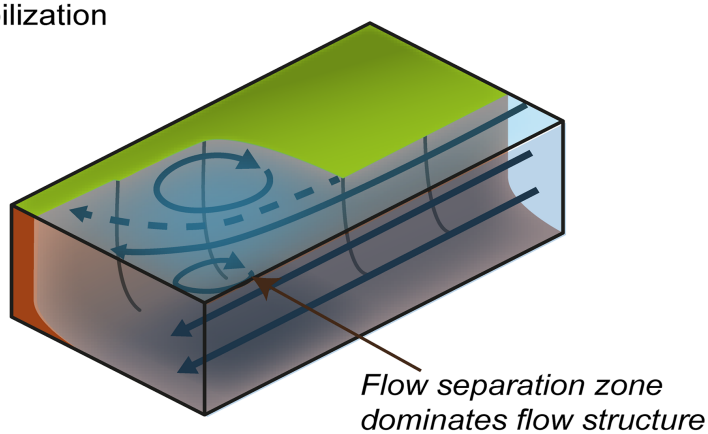


Stage IV: Embayment subsumation

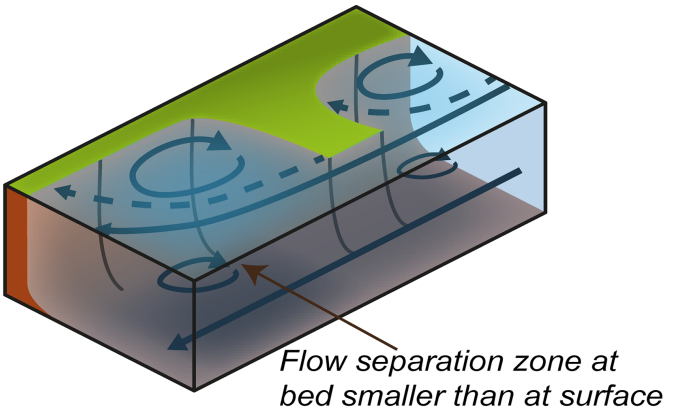

*Geophysical Research Letters*

Supporting Information for

# Modulation of outer bank erosion by slump blocks: disentangling the protective and destructive role of failed material on the three-dimensional flow structures.

Christopher Hackney[1], Jim Best[2], Julian Leyland[1], Stephen E. Darby[1], Daniel R. Parsons[3], Rolf Aalto[4], Andrew Nicholas[4]

[1]Geography and Environment, University of Southampton, SO17 1BJ, UK.

[2]Departments of Geology, Geography and GIS, Mechanical Science and Engineering and Ven Te Chow Hydrosystems Laboratory, University of Illinois at Urbana Champaign, Champaign, IL 61820, USA.

[3]Geography, Earth and Environmental Sciences, University of Hull, HU6 7RX, UK.

[4]Rolf Aalto and Andrew Nicholas, University of Exeter, Geography, Exeter, EX4 4RJ UK.

## Contents of this file



## Additional Supporting Information (Files uploaded separately)



## Introduction

The supplementary material includes a text description of the methodology for calculating critical shear stresses of the bank material using the Cohesive Strength

Meter, the methodology used for calculating the boundary shear stresses derived from the ADCP data and figures showing examples of the velocity profiles extracted from the ADCP data. It also contains figures showing the location of individual ADCP transects within the two embayments identified in Figure 1 of the main text. Additionally, instantaneous vertical flow fields from an ADCP transect that was located closest to the slump block (~10 m downstream) in Embayment 1 are presented in Figure S5. Instantaneous vertical flow fields from a transect in the middle of Embayment 2 (without a slump block) are provided in Figure S6 for comparison. Fly-though videos of the embayments considered in this study are provided in Movies S1 and S4.

**Text 1**

Bank material critical shear stresses (N $m^{-2}$) were calculated using a Cohesive Strength Meter [CSM; *Paterson*, 1989; *Tolhurst et al.*, 1999; *Tolhurst et al.*, 2000]. The CSM operates in a similar fashion to jet testing devices., however, the CSM detects the onset of erosion by monitoring optical transmission within an opaque test chamber that houses the jet nozzle (1 mm internal diameter) and infrared transmitter and receiver diodes. Erosion is detected via falls in optical transmission induced by the suspension of sediment via the jet. A total of 45 repeat tests were conducted on the river bank near to Embayment 1 (Figure S3). The distribution of the resulting critical shear stresses (Figure S1) was analyzed and the mean critical shear stresses (0.6 N $m^{-2}$) and the standard deviation of the samples (0.3 N $m^{-2}$) was calculated. The entire distribution is shown in Figure S1. It is noted that 11 of these samples (26% of the total) have critical shear stresses of 0.4 N $m^{-2}$ or less. This value represents the maximum value of shear stress extracted from aDcp data in Figure 3 of the main text, therefore it is likely that during the flow stage observed here some bank erosion was occurring.

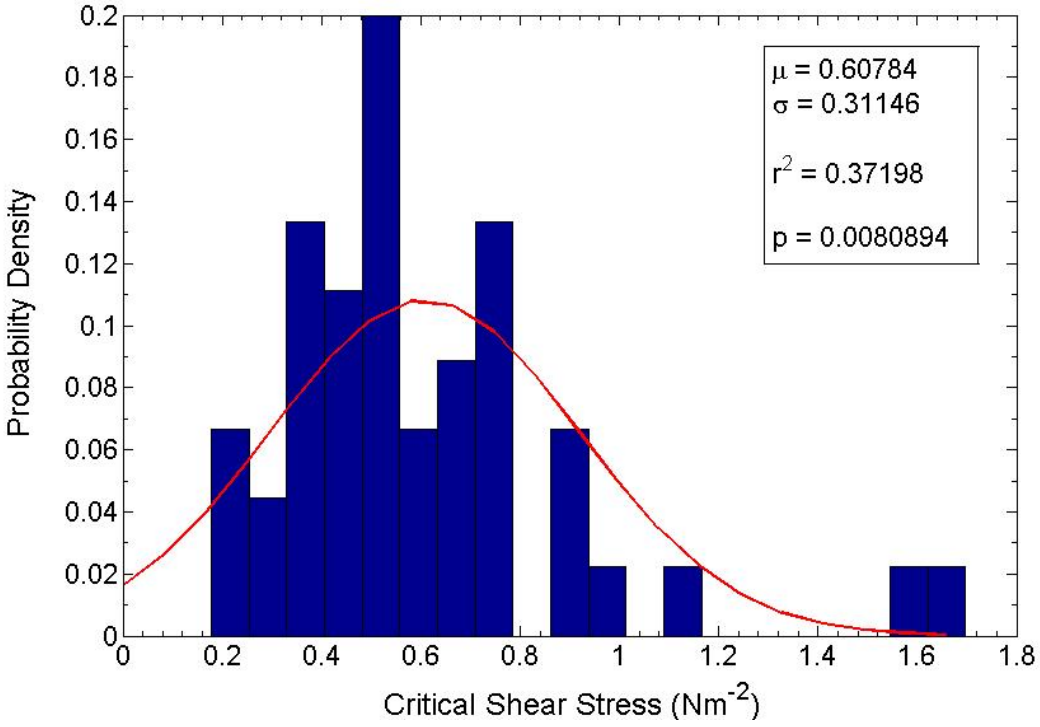


**Figure S1.** Distribution and fit statistics (for a Gaussian curve) of critical shear stresses of the bank material as obtained using the Cohesive Strength Meter (CSM). The total number of CSM measurements acquired at this site was 45.

Boundary shear stresses were derived from the velocity gradient *m* calculated using a least-squares regression between *ln(z)* and *u*, where *u* is the velocity at elevation *z* above the bed, for each vertical ensemble within each ADCP transect. This was fitted to the logarithmic portion of the velocity profile, which was determined through analysis of the individual velocity profiles. The shear velocity, $u_*$, was calculated as:

$$u_* = \kappa m$$

where $\kappa$ is the von Karman constant equal to 0.41 and the boundary shear stress, $\tau$, was calculated as:

$$\tau = \rho u_*^2$$

where $\rho$ is the density of water (kg $m^{-3}$). We do this for velocity profiles through the water column. All regressions exclude data in the lower 6% of the flow where acoustic sidelobe interference affects the accuracy of the velocity estimates.

Examples of the velocity profiles extracted from the ADCP are show in Figures S2 and S3. These figures highlight the logarithmic boundary layer near the base of the flow is present both close to the bank, and further out in the main channel. This permits the use of the log-law to estimate shear velocity. We do note, that alternative methodologies [e.g. *Vermeulen et al.*, 2011] would enable the calculation of Reynolds stresses.

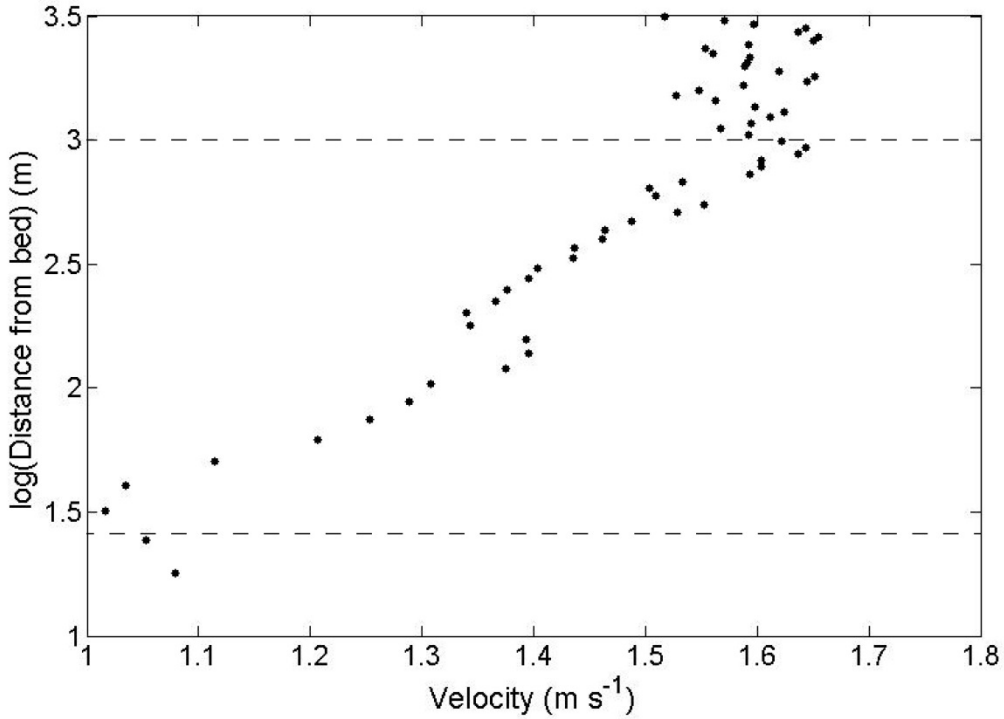


**Figure S2.** Velocity profile extracted from the ADCP data at transect 1C approximately 150 m from the bank. The dashed lines delineate the area in which the log-law calculations of shear stress were derived.

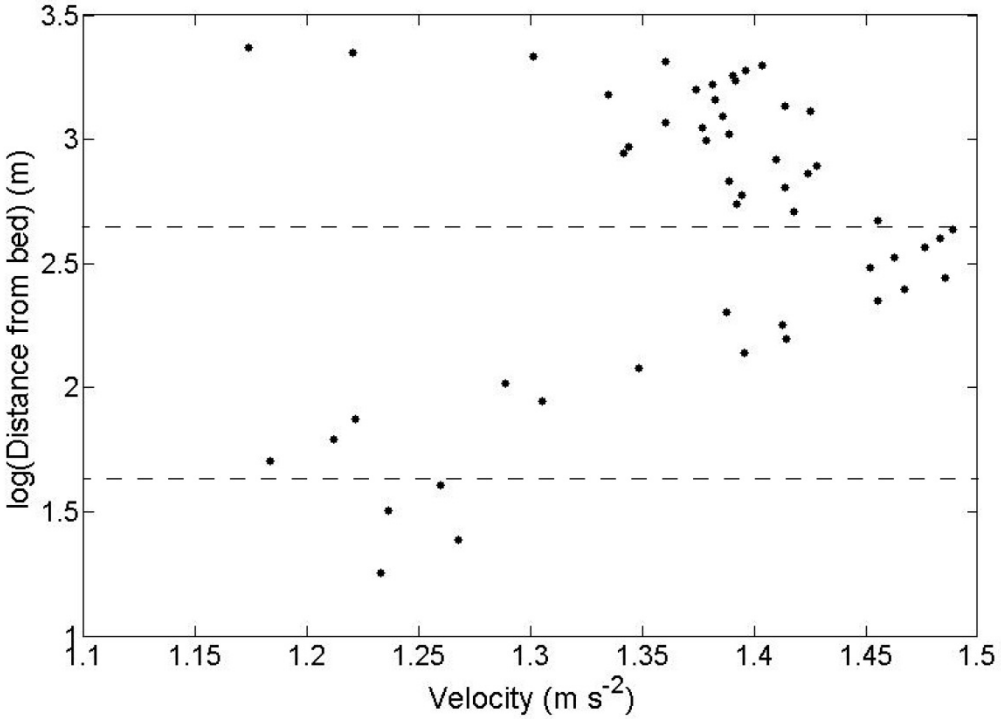


**Figure S3.** Velocity profile extracted from the ADCP data at transect 1D approximately 30 m from the bank. The dashed lines delineate the area in which the log-law calculations of shear stress were derived.

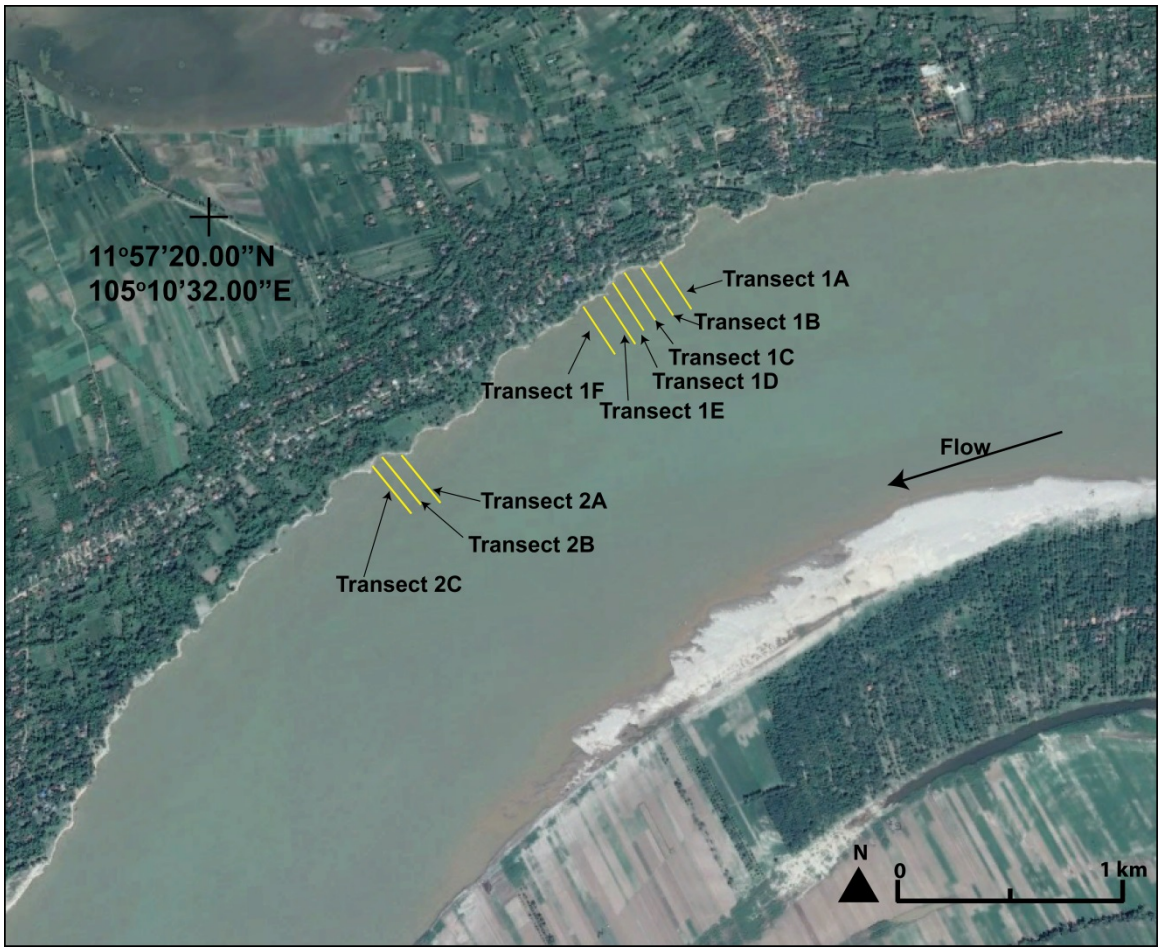


**Figure S4.** Location of the individual ADCP transects and ADCP transect numbers.

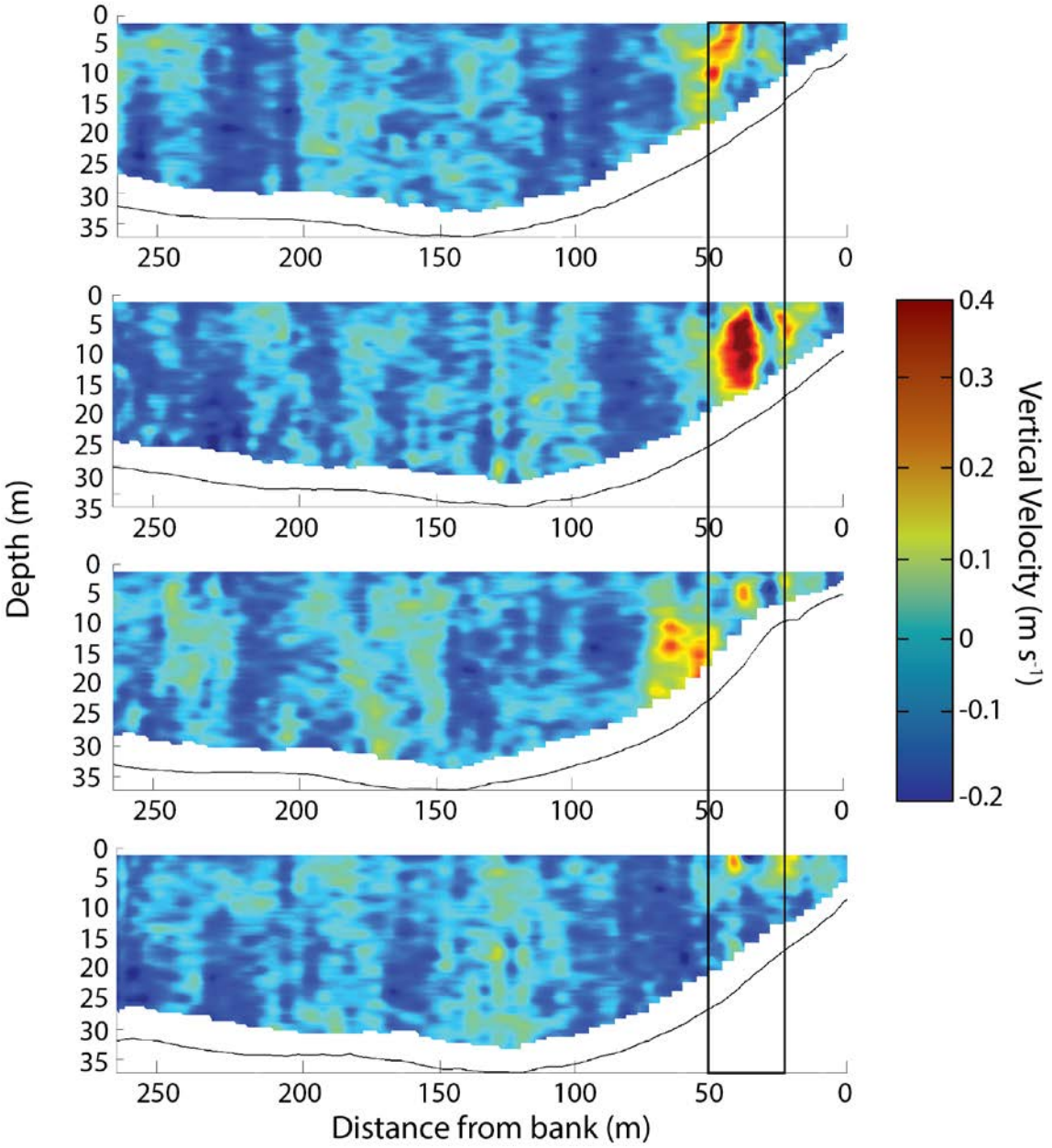


**Figure S5.** Instantaneous vertical velocities (m $s^{-1}$) captured by the individual ADCP passes conducted at location Transect 2D (Figure S1) that was located 10 m downstream of the slump block in Embayment 1. The box bounding 20 – 50 m from the bank (located on the right hand side of each diagram) defines the width of the slump block 10 m upstream of the transects reported here. The outer bank is on the right hand side of each diagram.

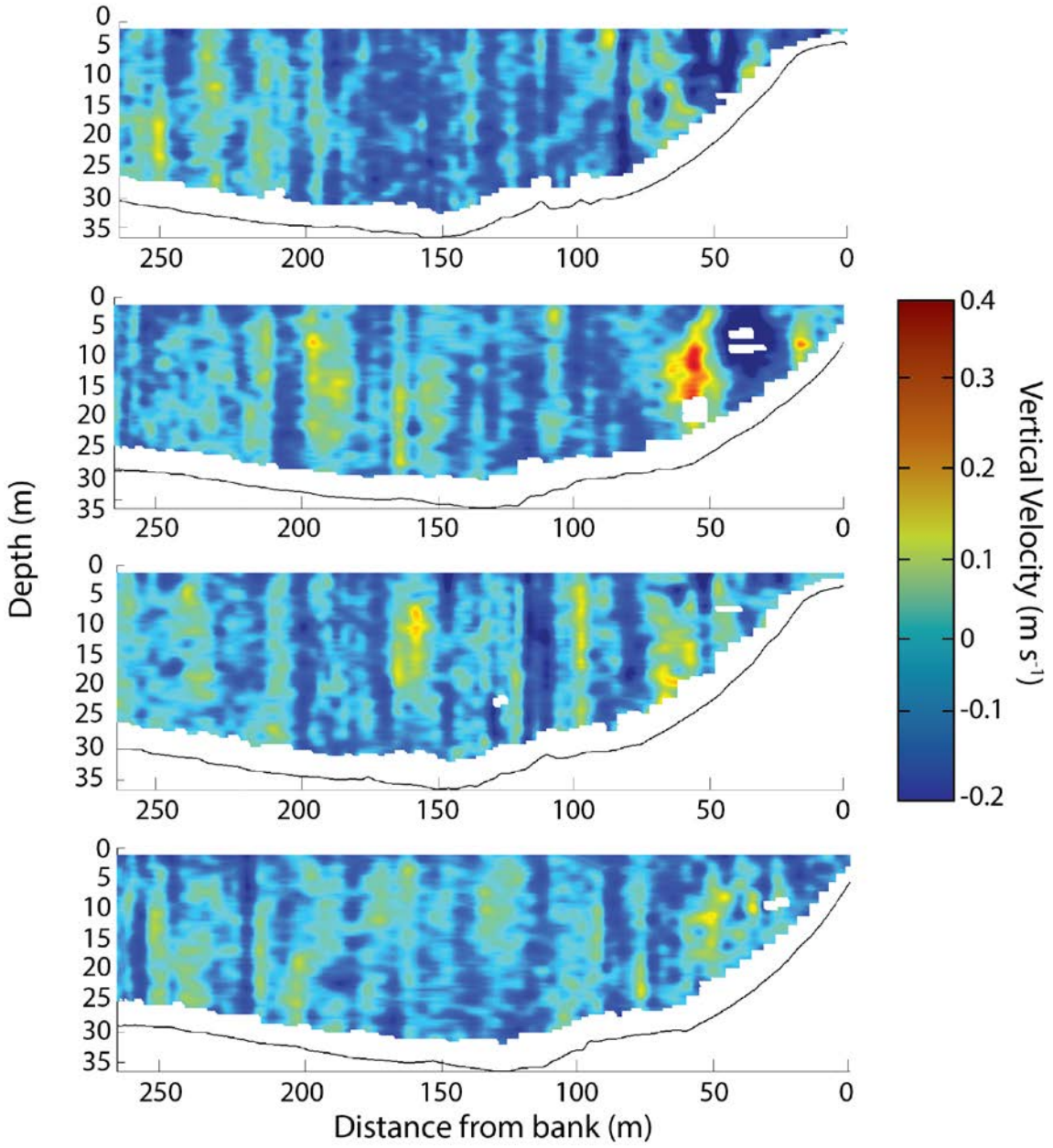


**Figure S6**. Instantaneous vertical velocities (m $s^{-1}$) captured by the individual ADCP passes conducted at location Transect 2B (Figure S1) that is located in the middle of Embayment 2, without a slump block. The outer bank is on the right hand side of each diagram.

**Movie S1.** Animated fly-though of Embayment 1 highlighting the presence of the submerged slump block in the centre of the embayment. Topographic data is the raw point cloud obtained from the terrestrial laser scanner and multibeam echo sounder surveys.

**Movie S2.** Animated fly-though of Embayment 1 with the vertical flow fields derived from the aDcp data overlain. Topographic data is the raw point cloud obtained from the terrestrial laser scanner and multibeam echo sounder surveys.

**Movie S3.** Animated fly-though of Embayment 2. Topographic data is the raw point cloud obtained from the terrestrial laser scanner and multibeam echo sounder surveys.

**Movie S4.** Animated fly-though of Embayment 2 with the vertical flow fields derived from the aDcp data overlain. Topographic data is the raw point cloud obtained from the terrestrial laser scanner and multibeam echo sounder surveys.

**References**

Paterson, D.M (1989), Short term changes in the erodibility of intertidal cohesive sediments related to the migratory behavior of epipelic diatoms, *Limnol. Ocenanogr., 34*(1), 223- 234, doi:10.4319/lo.1989.34.1.0223

Tolhurst, T.J., K.S. Black, S.A. Shayler, S. Mather, I. Black, K. Barker and D. M. Paterson (1999), Measuring the in situ erosion shear stress of intertidal sediments with the cohesive strength meter (CSM), *Estuarine Coastal Shelf Sci., 49*, 281 – 294, doi:10.1006/ecss.1999.0512.

Tolhurst, T.J., K.S. Black, D.M. Paterson, H.J. Mitchener, G.R. Termaat and S.A. Shayler (2000), A comparison and measurement standardization of four in situ devices for determining the erosion shear stress of intertidal sediments, *Cont. Shelf Res., 20*, 1397 – 1417, doi:10.1016/S0278-4343(00)00029-7.

Vermeulen, B., A.J.F. Hoitink and M.G. Sassi (2011), Coupled ADCPs can yield complete Reynolds stress tensor profiles in geophysical surface flows, *Geophysical Research Letters,* 38, L06406, doi:10.1029/2011GL046684.